

Variation of the $\gamma\gamma$ opacity by the He II Lyman continuum constrains the location of the γ -ray emission region in the blazar 3C 454.3

Boris E. Stern^{1,2*} and Juri Poutanen^{3*}

¹*Institute for Nuclear Research, Russian Academy of Sciences, Prospekt 60-letiya Oktyabrya 7a, Moscow 117312, Russia*

²*Astro Space Center, Lebedev Physical Institute, Profsoyuznaya 84/32, Moscow 117997, Russia*

³*Astronomy Division, Department of Physics, PO Box 3000, FIN-90014 University of Oulu, Finland*

Accepted 2011 June 29. Received 2011 June 29; in original form 2011 May 13

ABSTRACT

We study spectral properties of the brightest γ -ray blazar 3C 454.3 using 138 weeks of observations by the *Fermi Gamma-ray Space Telescope (Fermi)*. We probe the behaviour of the source as a function of time at different brightness levels. The *Fermi* spectra in the GeV range can be well described by a wide underlying lognormal distribution with the photon-photon absorption breaks produced by the He II and H I Lyman recombination continua (LyC). We find a power-law dependence of the peak energy on flux and discover anti-correlation between the column density of the He II LyC and flux. This implies that the γ -ray emission zone lies close to the boundary of the high-ionization part of the broad-line region and moves away from the black hole when the flux increases. Identification of the γ -ray production with the relativistic jet, implies that the jet is already accelerated at sub-parsec distances from the central black hole, which favours the Blandford-Znajek process as the jet launching mechanism.

Key words: black hole physics – galaxies: active – galaxies: jets – gamma rays: observations – quasars: emission lines – quasars: individual (3C 454.3)

1 INTRODUCTION

The flat spectrum radio quasar (FSRQ) 3C 454.3 at redshift $z = 0.859$ is by far the brightest blazar in the γ -ray range during the lifetime of the *Fermi Gamma-ray Space Telescope (Fermi)*. Since the start of operation in August 2008 the *Fermi* Large Area Telescope (LAT) has detected more than hundred thousand photons from this object. Its brightness has been changing by at least two orders of magnitude (see Fig. 1): after a bright state in 2008, the blazar turned to a very low state in the spring of 2009, then the flux has been gradually increasing. The bright flares then occurred in November 2009 and April 2010 and the brightest γ -ray flare ever observed from a blazar happened in November 2010.

The early data from the first 160 days of the *Fermi* observations have demonstrated a clear spectral break around 2.5–3 GeV (Abdo et al. 2009). Similar breaks in the GeV range have been observed in several other FSRQs and low-synchrotron peak BL Lac objects (Abdo et al. 2010). Later works by Ackermann et al. (2010) and Abdo et al. (2011) dedicated to 3C 454.3 found the spectral hardness–flux correlation at a nearly constant break energy. First interpretations of the breaks invoking the external Compton mechanism with a truncated electron spectrum (Abdo et al. 2009; Finke & Dermer 2010) do not reproduce as sharp a break as observed. The stability of the break energy favours instead the absorption of the GeV photons by the photon-photon ($\gamma\gamma$) pair production

on the He II and H I Lyman recombination continua (LyC) from the broad-line region (BLR), as proposed by Poutanen & Stern (2010, hereafter PS10). A relatively high opacity in the He II LyC observed in a number of bright blazars implies the location of the γ -ray emitting region within the highly ionized inner part of the BLR.

Motivated by the extremely rich photon statistics from 3C 454.3, in the present work we particularly try to answer the following questions:

- (i) Is the spectral break consistent with the $\gamma\gamma$ -absorption on the He II LyC at various source fluxes? We do not have a freedom of choosing the position of the break, with the only free parameter being the LyC column density. A good fit at a rich statistics would be a strong argument in favour of the absorption hypothesis.
- (ii) Is there any correlation between the break sharpness (i.e. absorption opacity in our interpretation) and the flux? If yes, then this would imply a varying location of the γ -ray emitting region.
- (iii) What is a proper characterization of the spectrum below the break? In PS10 the hypothesis for the underlying (unabsorbed) spectrum was a power-law. The underlying spectrum can actually be slightly curved with respect to the power-law.

2 DATA AND THEIR ANALYSIS

The light curve of 3C 454.3 from the start of the *Fermi* data records to 2011 April 1 is shown in Fig. 1. We split the data into ten time intervals covering periods of more or less constant flux levels and

* E-mail: stern.boris@gmail.com, juri.poutanen@oulu.fi

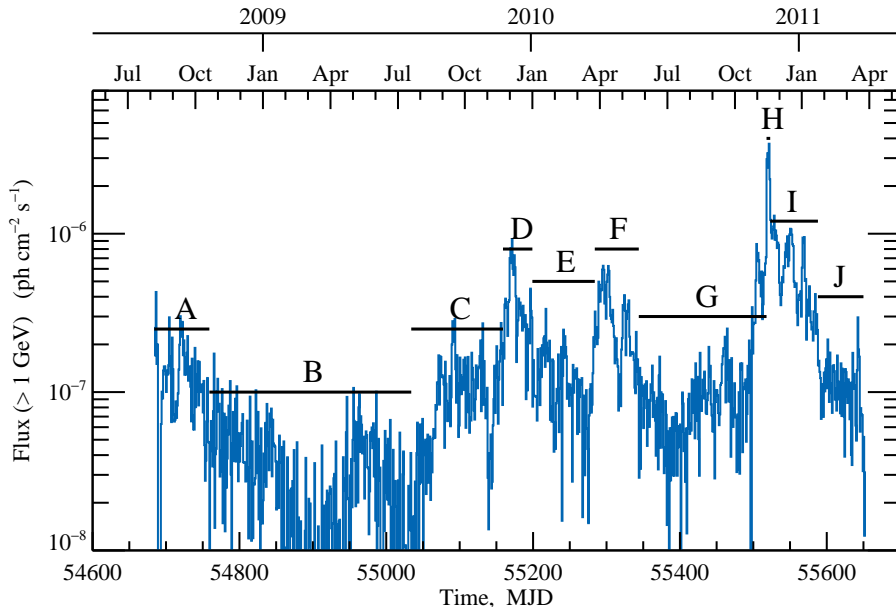


Figure 1. The light curve of the γ -ray blazar 3C 454.3 from the beginning of the *Fermi* data records to 2011 April 1. Horizontal bars mark the time intervals used in the spectral analysis (see Table 1).

analyze the spectrum in each interval. We use our own software for the data analysis because the standard software distributed by the *Fermi* LAT team does not contain the required spectral models. The energy-dependent exposure function was calculated using the spacecraft pointing history:

$$\text{Exposure}(E, \Delta T) = \int_{\Delta T} S(E, \theta(t)) dt, \quad (1)$$

where ΔT is the time interval of interest, θ is the angle between the detector axis and the direction to the object and $S(E, \theta)$ is the detector effective area at energy E . The spectral models folded with the exposure function are fitted to the observed counts in 13 logarithmically spaced energy bins in the energy range 0.15–60 GeV.

We included the events of classes 3 and 4 and imposed the cuts at zenith angle $< 105^\circ$. We used P6_V3_DIFFUSE version of the response function. The background was measured in a circle with the radius 6° , separated from the object by $\sim 15^\circ$ and avoiding local sources. We accumulate counts in the circle centered at the source location with the energy-dependent radius $r = \max\{10^\circ (E/100 \text{ MeV})^{-0.7}, 0.6^\circ\}$ (which corresponds to 95% containment). Statistical errors were treated as Gaussian, except in a few bins at higher energies, where the number of photons is low, we use Poisson likelihood adding $-2 \ln P(n, \mu)$ to χ^2 (here n is the number of counts in the bin and μ is the prediction of the model). The number of such bins is small and the meaning of χ^2 is not significantly affected. For the minimization we use the standard code MINUIT from the CERN library. We checked that our software reproduces within statistical errors the results of the *glike* task for standard spectral models such as power-law and broken power-law (compare table 2 in PS10 with table 1 in Abdo et al. 2010). Fig. 2(a) presents the spectra of 3C 454.3 accumulated in each time interval.

3 SPECTRAL FITS

First, we fit the data with a simple power-law model. This is our first null-hypothesis against which we check the significance of the

break. The resulting values of χ^2 are given in column 3 of Table 1. Then we add the $\gamma\gamma$ -absorption by photons in two “lines” at 54.4 and 13.6 eV (double absorber model, DA), which correspond to the energies of the He II and H LyC, which are the strongest features in the BLR spectra at relevant energies. These continua are basically line-like because the photoionized region temperature is typically much below the corresponding ionization potentials of H and He. Within this model, the spectral breaks are expected at the energies $261/(E_{\text{line}}(\text{eV})[1+z])$ GeV corresponding to the threshold of the $\gamma\gamma$ absorption on photons of energy E_{line} and redshifted. In 3C 454.3, the breaks should appear at 2.6 and 10.3 GeV, which is consistent with observations (Abdo et al. 2009; Ackermann et al. 2010; PS10; see Fig. 2).

The absorption strength by the isotropic line photons is parameterized by the Thomson optical depth (see PS10):

$$\tau_T = N_{\text{ph}} \sigma_T \approx 110 \frac{L_{\text{line},45}}{R_{18}} \frac{10 \text{ eV}}{E_{\text{line}}}, \quad (2)$$

where N_{ph} is the photon column density along the line of sight, σ_T is the Thomson cross-section, L_{line} is the line luminosity, and R is the typical size. (We defined $Q = 10^x Q_x$ in cgs units.) The energy-dependent opacity $\tau_{\gamma\gamma}(E, E_{\text{line}})$ is obtained by multiplying τ_T by the angle-averaged $\gamma\gamma$ cross-section in units of σ_T , which has a maximum of ~ 0.2 at three times the threshold energy (see Aharonian 2004; PS10). The opacities produced by two “lines”, τ_{He} and τ_{H} , were free parameters. We see that with the power-law null-hypothesis all spectra have very significant breaks and require non-zero absorption opacities (column 4 in Table 1). However, the residual value of χ^2 is still high for many spectra, especially for the average spectrum corresponding to the entire observational period, mostly because of the spectral curvature below the break.

The simplest way to account for this curvature is to replace the power-law null-hypothesis by the lognormal distribution (or “log-parabola”, which is essentially the same function in a different representation, see Massaro et al. 2004, Ackermann et al. 2010), which we use in the decimal form

$$EF_E \propto 10^{-\log^2(E/E_{\text{peak}})/\sigma_{\text{ln}}^2}. \quad (3)$$

Table 1. Spectral properties of 3C 454.3.

Interval	Dates ^a MJD	χ^2/dof				σ_{ln}^d	F^e	E_{peak}^f MeV	τ_{He}^f	τ_{H}^f	χ^2/dof^f
		Power-law	PL + DA ^b	Lognormal	Logn + DA ^c						
A	54684–54759	84/12	7.7/10	37/11	7.7/9	>4 ^g	2.8	32±6	3.2 ^{+1.0} _{-0.9}	21 ⁺²⁹ ₋₁₄	16/10
B	54759–55034	34/12	8.4/10	16/11	7.3/9	3.3 ^{+0.9} _{-0.7}	0.68	11±3	4.5 ^{+1.3} _{-1.2}	0.4 ^{+7.0} _{-0.4}	7.5/10
C	55034–55159	65/12	6.8/10	16/11	3.7/9	3.2±0.6	2.4	15±3	4.0±0.9	3.1 ^{+8.3} _{-3.0}	3.8/10
D	55159–55199	81/12	6.7/10	14/11	2.9/9	3.1 ^{+1.0} _{-0.4}	9.1	49±6	2.8±0.7	4.6 ^{+3.0} _{-2.7}	3.2/10
E	55199–55284	63/12	40/10	4.4/11	4.4/9	1.6±0.1	3.0	23±4	4.0±1.0	3.9 ^{+5.5} _{-3.9}	19/10
F	55284–55344	112/12	23/10	27/11	17/9	2.9 ^{+0.5} _{-0.3}	7.6	33±5	2.6±0.6	4.0 ^{+2.7} _{-2.1}	17/10
G	55344–55517	85/12	13/10	18/11	7.9/9	3.2 ^{+0.7} _{-0.5}	3.4	19±3	2.1±0.6	3.1 ^{+2.4} _{-2.0}	8.8/10
H	55517–55522	79/12	18/10	11/11	5.9/9	2.6 ^{+0.2} _{-0.3}	55	126±17	1.6±0.6	7.3 ^{+2.8} _{-2.5}	6.8/10
I	55522–55587	242/12	33/10	28/11	10/9	2.5±0.2	15	60±5	2.7±0.4	5.2 ^{+2.6} _{-1.5}	11/10
J	55587–55652	43/12	11/10	13/11	7.2/9	2.4 ^{+0.6} _{-0.4}	2.6	26±6	3.1 ^{+1.3} _{-1.1}	>8 ^g	7.3/10
A+C+E+G		315/12	33/10	42/11	9.0/9	2.7±0.2	2.9	20±2	3.2±0.4	6.2 ^{+2.2} _{-1.8}	9.0/10
D+F+I		565/12	56/10	71/11	23/9	2.8 ^{+0.3} _{-0.2}	11	48±3	2.7±0.3	7.2±1.5	23/10
A–J	54684–55652	1099/12	85/10	129/11	23/9	2.6±0.2	3.9	35±2	2.7±0.2	8.1 ^{+1.5} _{-1.2}	23/10

^aThe start and the end of the interval. ^bPower-law plus double absorber (DA) model. ^cLognormal plus DA model. ^dBest-fitting values of σ_{ln} for the lognormal + DA model. ^eFlux EF_E at 1 GeV in units of 10^{-10} erg cm⁻² s⁻¹. ^fBest-fitting values of E_{peak} , τ_{He} and τ_{H} and the corresponding χ^2/dof for the lognormal (with $\sigma_{\text{ln}} = 2.7$) + DA model. ^g1 σ lower limit.

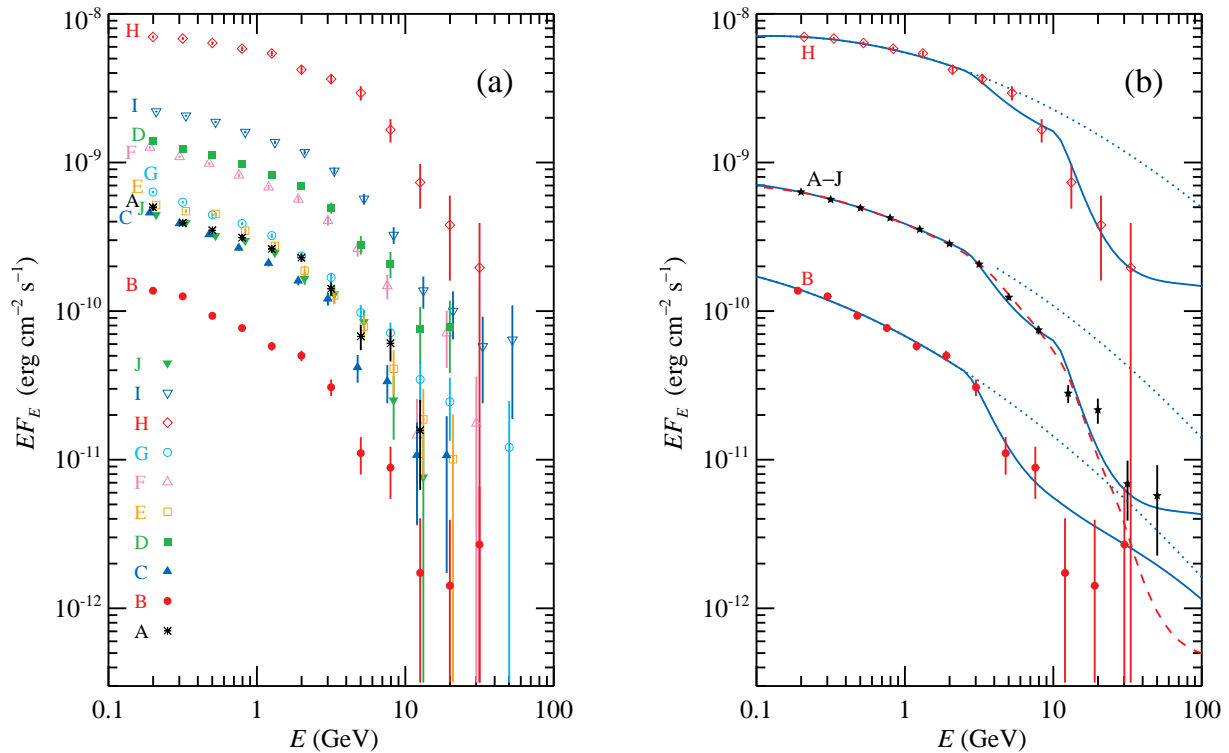


Figure 2. (a) Spectral energy distribution (SED) of 3C 454.3 for ten intervals A–J. (b) SED of 3C 454.3 for intervals B and H of the lowest and highest fluxes as well as averaged over the whole observation period of 2.5 years (sum of intervals A–J). The solid curves show the best-fitting lognormal ($\sigma_{\text{ln}} = 2.7$) + DA model. The dashed curve represents the fit with the lognormal distribution absorbed by BLR at a fixed ionization parameter $\log \xi = 2.5$ (see PS10). The dotted curves show the unabsorbed lognormal distributions.

The resulting fits are shown in columns 5 (without absorption) and 6 (with DA) of Table 1. We see a significant decrease in χ^2 compared to the power-law-based models. The DA model gives a substantial reduction in χ^2 in all cases (except for interval E). These fits are superior compared to any simple phenomenological model considered earlier (e.g. lognormal, broken power-law, or an exponentially cutoff power-law, see Abdo et al. 2011).

If the spectral break is indeed caused by the $\gamma\gamma$ -absorption on the He II LyC, its position should be stable. In that case we can expect that the break should become more significant in the average spectrum corresponding to the whole observation period. Indeed, this is the case, the lognormal distribution without absorption fits the data (see Table 1) at $\chi^2 = 129$ for 11 degrees of freedom (dof). The DA improves the fit (see Fig. 2(b)), but the residual

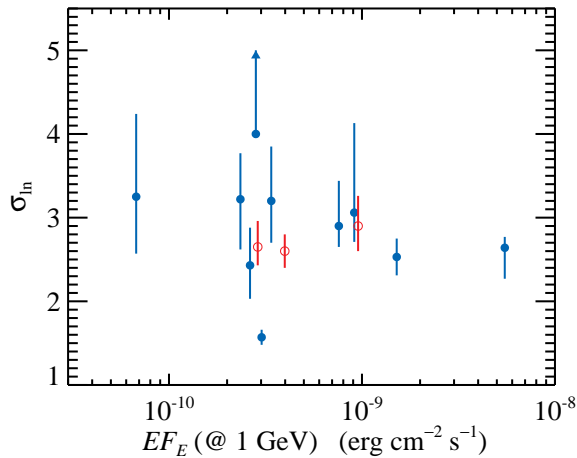


Figure 3. Dependence of the width of the best-fitting lognormal + DA model on flux at 1 GeV. The parameters for the intervals A+C+E+G, A–J and D+F+I are shown by open circles.

value $\chi^2/\text{dof} = 22.8/9$ is still high. The absorption model for the BLR at a fixed ionization parameter $\log \xi = 2.5$ (see PS10) gives $\chi^2/\text{dof} = 27/10$, with the quality of the fit being better ($\chi^2/\text{dof} = 7/7$) in the range <15 GeV. The main contribution to the residual χ^2 comes actually from the high-energy tail of the spectrum and might have a simple interpretation: the absorber optical depth varies during the observation and the sum of the spectra with low and high opacities differs from the spectrum at a fixed intermediate opacity.

The best-fitting value of σ_{ln} is nearly constant $\sim 2.5\text{--}3$ (see column 7 of Table 1 and Fig. 3), with the interval E being again an outlier. In order to avoid extra statistical noise, we fix $\sigma_{\text{ln}} = 2.7$ and then probe the correlation of other parameters with the source brightness (see Table 1). We find a highly significant correlation of the peak energy E_{peak} with flux, which is well represented by a power-law (Fig. 4):

$$E_{\text{peak}} = (46 \pm 2) F_{-9}^{0.60 \pm 0.04} \text{ MeV}, \quad (4)$$

where $F = EF_E$ at 1 GeV. This confirms a previously known hardness–flux correlation (Ackermann et al. 2010). We also observe a marginally significant (2.5σ) anti-correlation between the $\gamma\gamma$ -opacity by the He II LyC and the flux (see Fig. 5):

$$\tau_{\text{He}} = (2.61 \pm 0.22) - (1.15 \pm 0.47) \log F_{-9}. \quad (5)$$

The opacity τ_{H} in the H I LyC does not vary significantly.

4 DISCUSSION AND SUMMARY

The BLRs around quasars emit a number of lines associated with very different ionization stages, with the high-ionization lines being broader (Peterson & Wandel 1999). Reverberation mapping demonstrated a strong anti-correlation between the line width and the time delays of the line response to the continuum variations (Peterson & Wandel 2000). All this implies strong stratification of the BLR that extends over two orders of magnitude in distance (Krolik 1999; Osterbrock & Ferland 2006). The BLR size, as measured from the C IV $\lambda 1549$ line delays, scales with the accretion luminosity as $R_{\text{CIV}} \approx 0.2 L_{47}^{1/2}$ pc (Kaspi et al. 2007). However, the delays in the high-ionization He II $\lambda 1640$ line are 3–5 times smaller in Seyferts (Korista et al. 1995; Peterson & Wandel 1999),

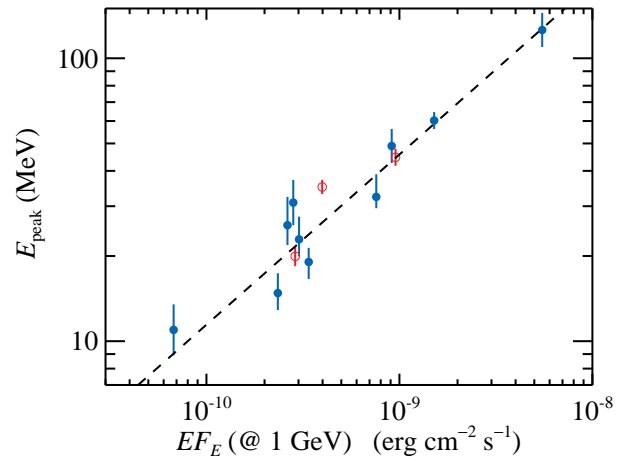


Figure 4. Dependence of the peak (in EF_E) of the best-fitting lognormal (with $\sigma_{\text{ln}} = 2.7$) + DA model on flux at 1 GeV. The dashed line shows the best-fitting relation for intervals A–J given by Equation (4). The parameters for the intervals A+C+E+G, A–J and D+F+I are shown by open circles.

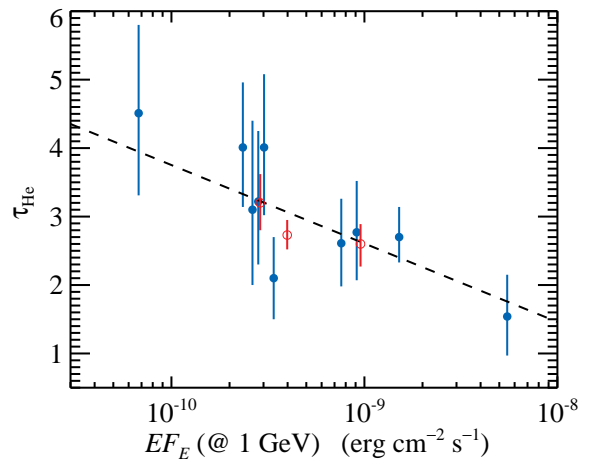


Figure 5. Dependence of the Thomson optical depth in the He II LyC (defined by Equation (2)) on flux at 1 GeV. The model and notations are the same as in Fig. 4. The dashed line shows the best-fitting relation for intervals A–J given by Equation (5).

while the Balmer lines give sizes 2–3 times larger. As the opacity in the GeV range depends on the line compactness (L/R), models assuming that all lines are produced at the same distance from the central source (e.g. Liu & Bai 2006; Reimer 2007), strongly underestimate the $\gamma\gamma$ -opacity by the relatively weak, high-ionization lines produced in a small volume (if the γ -rays are produced closer to the centre) and overestimate the opacity for multi-GeV photons from the strong, low-ionization lines which are produced much further away than the fiducial distance obtained from C IV.

A high average γ -ray luminosity of 3C 454.3 during the last two years with flares up to $L_{\gamma} \sim 2 \times 10^{50}$ erg s $^{-1}$ (Abdo et al. 2011) provided an order of magnitude increase in photon statistics compared to the earlier data analysed by Abdo et al. (2009) and PS10. It became even more evident that the spectral breaks at ~ 3 GeV are real. The spectra at all fluxes are well described by a log-normal distribution absorbed by the He II and H I LyC at 54.4 and 13.6 eV. The fits with this model are superior compared to the previously used simple phenomenological models, especially at high fluxes with high photon statistics.

The BLR size corresponding to the He II and H I LyC can be estimated from Equation (2):

$$R_{\text{He}} \approx 0.22 L_{\text{He},44}(\tau_{\text{He}}/3) \text{ pc}, \quad R_{\text{H}} \approx 3.7 L_{\text{H},45}(\tau_{\text{H}}/7) \text{ pc}. \quad (6)$$

Wills et al. (1995) report the luminosity of 3C 454.3 in Ly α of $\sim 10^{45}$ erg s $^{-1}$ and in He II $\lambda 1640$ of 6×10^{43} erg s $^{-1}$. Assuming equal luminosities in LyC and Ly α , the resulting R_{H} is much larger than the usually quoted sub-pc size of BLR, but is consistent with the absence of Ly α variability in powerful quasars (Kaspi et al. 2007). The He II LyC luminosity is probably larger than 10^{44} erg s $^{-1}$, but is model dependent and therefore the estimate of R_{He} is less certain. A rather large ratio $\tau_{\text{He}}/\tau_{\text{H}}$ (between about 1/4 and 1) and the observed τ_{He} -flux anti-correlation indicate that the γ -ray emission region lies close to the boundary of the He III zone at $R \lesssim R_{\text{He}}$ and moves out at higher luminosity. Absorption troughs at 0.3–0.7 GeV due to the high-ionization C and O lines are potentially detectable, but require high photon statistics and better calibration of LAT.

We note that the typical values of $\tau_{\text{He}} \sim 2\text{--}4$ imply that the maximum optical depth due to the He II LyC photons (at about 7 GeV – three times the threshold value of $4.8/(1+z)$ GeV) varies around 0.4–0.8. The absorption by He II LyC is very significant and accurately describes the data in the 3–15 GeV range. At high energies, the opacity decreases roughly inversely with the photon energy and becomes negligible above ~ 300 GeV. The opacity there is dominated by the optical/IR lines which are mostly produced in the low-ionization zone of BLR at large distances. This strongly reduces the opacity and can make the BLR transparent for the multi-GeV to TeV photons.

A probable excess of photons above 15 GeV (especially for the average spectrum) over the prediction of the model with the best-fitting absorption indicates that the spectrum is a superposition of emission states with different opacities due to the extended or moving emission zone. This proposal is supported by the spectral variability seen during the latest flare in November 2010 (Abdo et al. 2011), where photons above 10 GeV mostly arrive at the end of the flare, clearly indicating the position of the γ -ray emitting region further away from the black hole.

Our findings that the spectral peak of the underlying continuum strongly correlates with the flux, with the width of the lognormal distribution being roughly constant, indicate a more efficient acceleration at high fluxes. These variations might not be consistent with the interpretation of the spectral curvature as the Klein-Nishina reduction of the Compton scattering efficiency of the Ly α photons (Ackermann et al. 2010). This in turn would imply that the seed photon energy density is not dominated by the hydrogen Lyman continuum and line photons (in the high-ionization zone of the BLR the metal lines and the He II Lyman photons are actually more energetically important). Alternatively, the steady electron distribution is modified by inefficient cooling in the Klein-Nishina regime (Zdziarski & Krolik 1993; Moderski et al. 2005).

The GeV breaks observed in bright blazars still do not answer the question what is the γ -ray production mechanism. It can be Compton scattering of the accretion disc (Dermer & Schlickeiser 1993) or BLR photons (Sikora et al. 1994), or even the synchrotron radiation of relativistic pairs. The efficient means for particle acceleration can be provided by the photon breeding mechanism (Stern & Poutanen 2006, 2008).

A small distance to the beginning of the γ -ray emitting region is supported by the fast variability observed from 3C 454.3 (Tavecchio et al. 2010; Bonnoli et al. 2011). Association of the beamed γ -ray emission with a relativistic jet implies that the jet

is already accelerated at a sub-parsec distance from the black hole (i.e. at thousand Schwarzschild radii from the $\sim 10^9 M_{\odot}$ black hole, Bonnoli et al. 2011). This, in turn, argues against the jet launching mechanism by the accretion disc (Blandford & Payne 1982), with the only known alternative being the extraction of the black hole spin energy by the Blandford-Znajek process (Blandford & Znajek 1977; Komissarov et al. 2007).

ACKNOWLEDGMENTS

This research was supported by the Academy of Finland grant 127512 and the Magnus Ehrnrooth foundation. The research made use of public data obtained from the Fermi Science Support Center. We thank Gabriele Ghisellini, Chuck Dermer and Maxim Barkov for useful discussions.

REFERENCES

- Abdo A. A. et al., 2009, ApJ, 699, 817
 Abdo A. A. et al., 2010, ApJ, 710, 1271
 Abdo A. A. et al., 2011, ApJ, 733, L26
 Ackermann M. et al., 2010, ApJ, 721, 1383
 Aharonian F. A., 2004, Very high energy cosmic gamma radiation: a crucial window on the extreme Universe. World Scientific Publishing, River Edge, NJ
 Blandford R. D., Payne D. G., 1982, MNRAS, 199, 883
 Blandford R. D., Znajek R. L., 1977, MNRAS, 179, 433
 Bonnoli G., Ghisellini G., Foschini L., Tavecchio F., Ghirlanda G., 2011, MNRAS, 410, 368
 Finke J. D., Dermer C. D., 2010, ApJ, 714, L303
 Dermer C. D., Schlickeiser R., 1993, ApJ, 416, 458
 Kaspi S., Brandt W. N., Maoz D., Netzer H., Schneider D. P., Shemmer O., 2007, ApJ, 659, 997
 Komissarov S. S., Barkov M. V., Vlahakis N., Königl A., 2007, MNRAS, 380, 51
 Korista K. T. et al., 1995, ApJS, 97, 285
 Krolik J. H., 1999, Active galactic nuclei: from the central black hole to the galactic environment. Princeton University Press, Princeton, N. J.
 Liu H. T., Bai J. M., 2006, ApJ, 653, 1089
 Massaro E., Perri M., Giommi P., Nesci R., 2004, A&A, 413, 489
 Moderski R., Sikora M., Coppi P. S., Aharonian F., 2005, MNRAS, 363, 954
 Osterbrock D. E., Ferland G. J., 2006, Astrophysics of gaseous nebulae and active galactic nuclei. University Science Books, Sausalito, CA
 Pacciani L. et al. 2010, ApJ, 716, L170
 Peterson B. M., Wandel A., 1999, ApJ, 521, L95
 Peterson B. M., Wandel A., 2000, ApJ, 540, L13
 Poutanen J., Stern B., 2010, ApJ, 717, L118 (PS10)
 Reimer A., 2007, ApJ, 665, 1023
 Sikora M., Begelman M. C., Rees M. J., 1994, ApJ, 421, 153
 Stern B. E., Poutanen J., 2006, MNRAS, 372, 1217
 Stern B. E., Poutanen J., 2008, MNRAS, 383, 1695
 Tavecchio F., Ghisellini G., Bonnoli G., Ghirlanda G., 2010, MNRAS, 405, L94
 Wills B. J. et al., 1995, ApJ, 447, 139
 Zdziarski A. A., Krolik J. H., 1993, ApJ, 409, L33